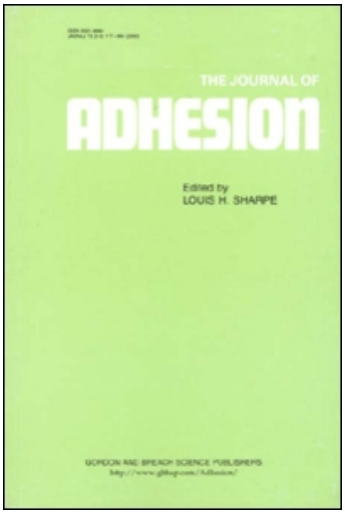

The Journal of Adhesion
Publication details, including instructions for authors and subscription information:
http://www.informaworld.com/smpp/title~content=t713453635

Elasto-Plastic Analysis of Adhesively Bonded Symmetric Single Lap Joints Under In-Plane Tension and Edge Moments

Jungmin Lee[a]; Hyonny Kim[b]
[a] Samsung SDI, Corporate R & D CAE Team, Kiheung, South Korea [b] Department of Structural Engineering, University of California - San Diego, La Jolla, California, USA

To cite this Article Lee, Jungmin and Kim, Hyonny(2007) 'Elasto-Plastic Analysis of Adhesively Bonded Symmetric Single Lap Joints Under In-Plane Tension and Edge Moments', The Journal of Adhesion, 83: 9, 837 — 870
To link to this Article: DOI: 10.1080/00218460701588158
URL: http://dx.doi.org/10.1080/00218460701588158

The Journal of Adhesion, 83:837–870, 2007

ISSN: 0021-8464 print/1545-5823 online
DOI: 10.1080/00218460701588158

Taylor & Francis
Taylor & Francis Group

Elasto-Plastic Analysis of Adhesively Bonded Symmetric Single Lap Joints Under In-Plane Tension and Edge Moments

Jungmin Lee
Samsung SDI, Corporate R & D CAE Team, Kiheung, South Korea

Hyonny Kim
Department of Structural Engineering, University of California – San Diego, La Jolla, California, USA

An analysis is presented that predicts adhesive shear and peel stresses and strains in an adhesively bonded single lap joint having symmetric configuration with adhesive behavior. The single lap joint is under tension loading together with moments induced by the interactions of the geometric eccentricity and the boundary conditions of the joint. The von Mises yielding criterion is used to relate the adhesive stress components within the yielded region. The adhesive strains are computed from the relative displacements of the adherends and can be considered as an average of the strain variation through the adhesive thickness direction. Example calculations show that the predicted adhesive shear and peel stress and strain profiles are well matched to detailed finite element analysis results. Generally, the analytical model predictions are found to be more accurate when the adhesive thickness is small.

Keywords: Beam on elastic foundation; Nonlinear adhesive; Shear-lag; Symmetric joint; Von Mises yielding criterion

INTRODUCTION

An analytical model is developed that predicts shear and peel stresses in adhesively bonded symmetric single lap joints while accounting for elastic-to-perfectly plastic adhesive behavior. The joints are loaded by both in-plane tension force and by moments induced from the

Received 25 July 2006; in final form 18 July 2007.

Address correspondence to Hyonny Kim, Department of Structural Engineering, University of California – San Diego, 9500 Gilman Drive #0085, La Jolla, CA 92093-0085, USA. E-mail: hyonny@ucsd.edu

geometric eccentricity of the joint. When the joint is symmetric, the shear and peel governing equations are decoupled and the edge moments can be calculated from joint geometry. The model computes shear stress based on shear lag assumptions and predicts peel stress using the beam on elastic foundation (BOEF) approach. Inside the elastic region, the governing equations are solved directly by using the linear constitutive relationship of the adhesive. The relationship between shear and peel stresses inside the plastic region is defined by the von Mises yielding model.

Classical analyses, based on shear-lag assumptions, have been previously developed to predict the adhesive shear stress in bonded joints of uniform bondline thickness for a symmetric joint with tension load only [1,2]. Improvements to the classical model include predicting peel stress [3–6], considering the asymmetry of the adherends [7–12], accounting for the effects of bondline thickness variation along the overlap dimension [13], and allowing for transverse shear deformation of the symmetric adherends [14].

Goland and Reissner [3] had first noticed the importance of the adhesive peel stress in addition to the adhesive shear stress in bonded lap joints. In order to solve the adhesive peel stress equation, a uniform rotation of the symmetric joint was assumed with corresponding edge moments computed from the joint geometry. Ojalvo and Eidinoff [4] and Oplinger [5] derived coupled governing equations based on plate theory in the manner first introduced by Goland and Reissner [3] and noted that the joint rotates nonlinearly as a function of the applied tension load. This rotation of the joint should generally be accounted for when calculating the moment boundary conditions.

Kline [6] presented a general joint analysis theory accounting for asymmetry of the joint adherends but provided a solution for only the symmetric case. Delale *et al*. [7] extended Goland and Reissner's approach for symmetric joints by formulating the adhesive shear stress equation to account for asymmetric adherends. However, the suggested edge moment boundary conditions by Delale *et al.* [7] results in a shear stress solution that does not equilibrate with the applied tension load. Approaches for the shear stress solution to asymmetric joints are presented by Yang and Pang [8], Bigwood and Crocombe [9], Mortensen and Thomsen [10] and Wu *et al.* [11] similarly do not balance applied force. Lee and Kim [12] presented a closed-form analytical elastic solution to the generally asymmetric joint that can consistently account for equilibrated edge moments and at the same time predicts a shear stress profile which is in force equilibrium with the applied loading. The aim of this article is to

extend the model to account for nonlinear material behavior of the adhesive, namely plasticity which develops prior to failure.

Adhesive plasticity before failure was accounted for in the analysis of symmetric scarf joints or single lap joints under in-plane shear load [15,16] and single lap joints under in-plane tension load [17–24]. The analysis of single lap joints under in-plane shear load is relatively simple because only adhesive shear stress needs to be considered. Nguyen and Kedward [15] suggested a two-parameter function to curve-fit the nonlinear adhesive constitutive behavior for use in adhesively bonded scarf joints. Kim and Lee [16] used the two-parameter fitting function to capture the nonlinearity of the adhesive behavior including softening after ultimate strength. The nonlinear adhesive shear governing equation was numerically solved to calculate the adhesive shear stress distribution in bonded symmetric single lap joints.

Hart-Smith [17] introduced an elastic-perfectly plastic subdivision of the adhesive joint to predict the adhesive shear stress and strain profiles. The Hart-Smith's elasto-plastic model [17] assumed that the ultimate shear stress and strain in the model were equal to the ultimate shear stress and strain of the real stress-strain curve of the adhesive, thereby maintaining the same strain energy. Pickett and Hollaway [18] adopted Hart-Smith's approach to determine the adhesive shear stress in fiber-reinforced plastic lap joints while computing adhesive peel stress using nonlinear finite element analysis (elastic-perfectly plastic behavior). The interaction of the peel and shear stresses in the yielded region was not investigated. Adams *et al.* [19] also adopted an approach accounting for nonlinear adhesive behavior that treats the peel stress as elastic-only.

Bigwood and Crocombe [20,21] pointed out the importance of the yielding model for the nonlinear adhesive problem. Secant modulus was used to correlate the three-dimensional stress and strain components over the whole adhesive constitutive behavior, hence the nonlinear adhesive problem was treated as an elastic problem with constantly varying modulus. Six first-order nonlinear differential governing equations were numerically integrated and all boundary conditions were initially assumed and then corrected iteratively. Comparison of their analytical solution with nonlinear finite element model calculations of the adhesive shear stress profile showed the analytical solutions to be accurate at the center portion of the joint. Under-prediction of the adhesive shear stress at the end of the joint reveals a concern, namely that the shear stress profile does not balance with the applied loading. Another iterative algorithm was suggested by Thomsen [22] for adhesively bonded tubular lap joints,

however, no validation to the suggested analytical model was provided.

Yang *et al.* [23] presented a simple closed-form model with an elastic-plastic adhesive. The J_2 flow rule and von Mises yielding criterion were used to predict the adhesive stress behavior in the yielded region. Adhesive shear stress in the plastic region was assumed to be dominant over all the other stress components, including peel stress. All adhesive stress components except adhesive shear stress were, thus, neglected.

A different approach by Tong [24,25] suggests an energy-based method to predict failure of the joint. The adhesive shear and peel governing equations were integrated to compute Modes I and II strain energy release rates. End-notched flexure adhesive specimens with the initial crack length, $\boldsymbol{a}$, were used to relate these calculations to failure loads. As presented, Tong's method [24,25] does not explicitly predict the adhesive stress profiles and the implementation of a fracture-based criterion is difficult to apply to bonded lap joint problems when the initial crack size is unknown, and in many cases does not exist prior to failure.

This article presents the development of a closed-form analytical model that accounts for elastic-perfectly plastic adhesive behavior in symmetric single lap joints. The independent adhesive stress components throughout the adhesive are computed in a manner such that force equilibrium is always satisfied. From the shear and peel stress, shear and peel strain profiles are also computed which can be used for failure assessment.

MODEL DESCRIPTION

The adhesively bonded symmetric single lap joint with all relevant geometric parameters is shown in Figure 1. The only externally

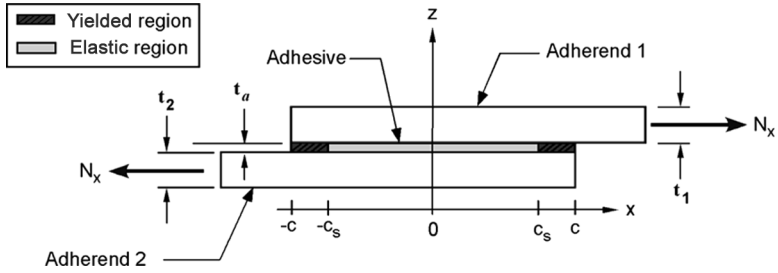

FIGURE 1 Single lap bonded joint.

applied load is the in-plane force per unit width, N_x. The following assumptions are made for the symmetric single lap joint:

- plane strain conditions ($\varepsilon_{yy} = \gamma_{xy} = \gamma_{yz} = 0$);
- adherends and adhesive have constant thickness;
- shear and peel stress is uniform through the adhesive thickness (z-direction);
- adherends do not deform due to transverse shear;
- linear elastic adherends;
- adhesive behaves as an elastic-to-perfectly plastic material;
- joint is symmetric—adherends are identical in thickness ($t_2 = t_1$) and material.

In Figure 1, the adhesive layer is subdivided into yielded and elastic regions. Since the joint is geometrically and materially symmetric, the yielded regions at both sides of the joint are the same size. As shown in Figure 2, boundary conditions are defined such that the joint is fixed at the left-end side ($x = -c$) against all movement and the in-plane tension load is applied to Adherend 1 at the right-end side ($x = c$), where the joint is free to move along the vertical direction but is constrained against the rotation. Therefore, at the boundaries, the transverse shear resultants $\overline{Q_1}$ and $\overline{Q_2}$ are zero, and the edge moments $\overline{M_1}$ and $\overline{M_2}$ are induced from the load path eccentricity. It has been shown that these edge moments can be computed from a simple geometric relationship when the joint is symmetric [12]. Note that the transverse displacements at $x = c$ was not constrained since real structures with significant unbonded length, *e.g.*, the thin skin of an aircraft in a single lap splice joint, would not have the same degree of transverse displacement constraint which exists when testing a lap joint in a test machine using rigid grips. However, to preserve consistency of the loading direction, the condition of no rotation was enforced.

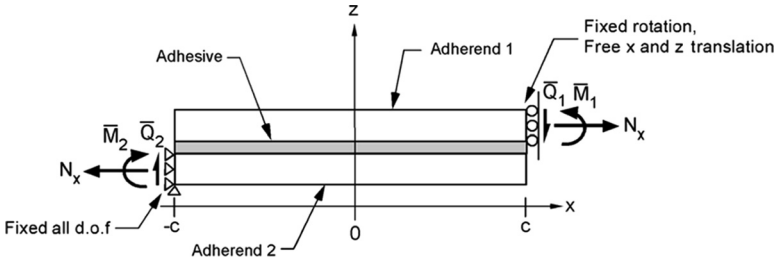

FIGURE 2 Boundary conditions.

Governing Equations

A differential slice, dx, of the joint at any location x is shown in Figure 3. The tangential (x-direction) and normal (z-direction) displacements at the interfaces of the adherends and the adhesive at $z_1 = 0$ and $z_2 = t_2$ are defined as u_1, w_1 and u_2, w_2, respectively. These adhesive-adherend interfacial displacements are a function of the in-plane axial stress resultants (N_1 and N_2), the internal moment resultants (M_1 and M_2), and the joint geometric and material parameters (thickness t, modulus E, and bending rigidity D) of the adherends. The adhesive shear strain, γ_{xz}^a, is determined from the interface-adjacent horizontal displacements, u_1 and u_2, and thickness, t_a, of

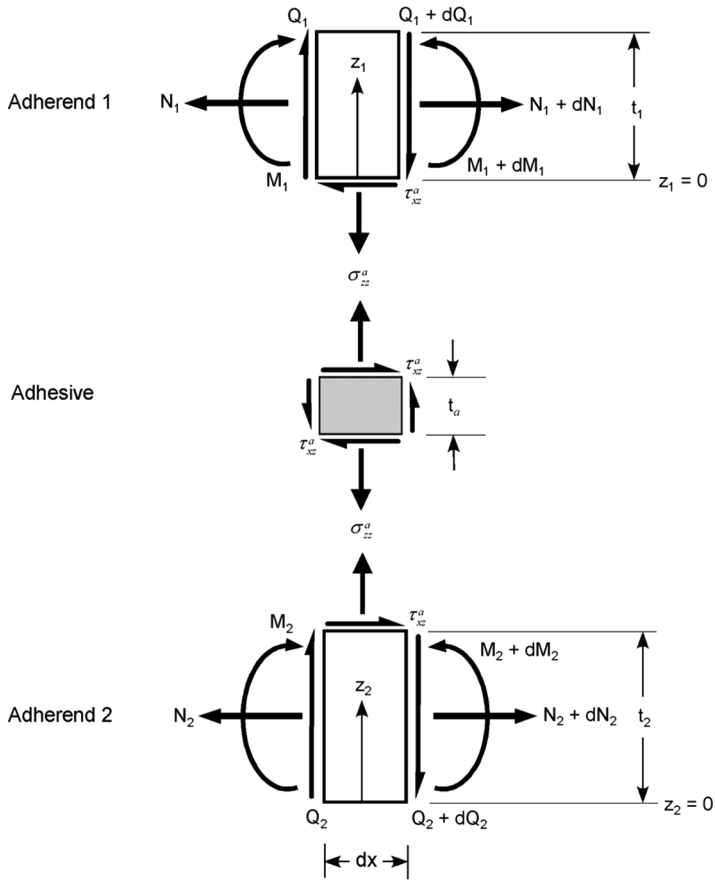

FIGURE 3 Differential element of single lap joint.

the adhesive:

$$\gamma_{xz}^{a} = \frac{1}{t_a}(u_1 - u_2). \tag{1}$$

Differentiating Eq. (1) with respect to x yields

$$\frac{d\gamma_{xz}^{a}}{dx} = \frac{1}{t_a}(\varepsilon_{x1} - \varepsilon_{x2}). \tag{2}$$

ε_{x1} and ε_{x2} are the x-directional normal strains in the adherends at the adhesive interface. These can be computed from the in-plane axial stress resultants (N_1 and N_2) and the internal moment resultants (M_1 and M_2) based on simple beam theory. Differentiating Eq. (2) with respect to x once more yields the relationship

$$\frac{d^2\gamma_{xz}^{a}}{dx^2} = \frac{1}{t_a}\left[\left(\frac{1}{E_1 t_1} + \frac{1}{E_2 t_2}\right) + \frac{1}{4}\left(\frac{t_1^2}{D_1} + \frac{t_2^2}{D_2}\right)\right]\tau_{xz}^{a} + \frac{1}{2t_a}\left(\frac{t_1}{D_1}Q_1 + \frac{t_2}{D_2}Q_2\right) \tag{3}$$

where τ_{xz}^{a} is the adhesive shear stress which can be shown to relate N_i, M_i, and Q_i *via* force and moment equilibrium applied to the differential slices shown in Figure 3 [12]. Also, E_i and D_i in Eq. (3) are the adherend elastic modulus and bending rigidity, respectively. The subscript i indicates Adherends 1 and 2. The sum of the transverse shear stress resultants within the adherends (Q_1 and Q_2) is zero when the joint is geometrically and materially symmetric [12]. For symmetric joints with $t_2 = t_1$, $E_2 = E_1$, and $D_2 = D_1$, Eq. (3) simplifies to

$$\frac{d^2\gamma_{xz}^{a}}{dx^2} = \frac{1}{t_a}\left[\frac{2}{E_1 t_1} + \frac{t_1^2}{2D_1}\right]\tau_{xz}^{a}. \tag{4}$$

Eq. (4) is the governing equation for shear strain in the adhesive. The adhesive peel stress, σ_{zz}^{a}, is determined from a beam on elastic foundation model by considering the two adherends as beams connected by a deformable interface. The relative transverse displacements, $\tilde{w}$, of the adherends are related as [12]

$$\frac{d^4\tilde{w}}{dx^4} = -\left(\frac{1}{D_1} + \frac{1}{D_2}\right)\sigma_{zz}^{a}, \tag{5}$$

where σ_{zz}^{a} is the adhesive peel stress. Eq. (5) can be written as a function of adhesive peel strain ε_{zz}^{a} *via* the relationship

$$\varepsilon_{zz}^{a} = \frac{1}{t_a}(w_1 - w_2) = \frac{\tilde{w}}{t_a}. \tag{6}$$

Substituting Eq. (6) into Eq. (5) yields

$$\frac{d^4\varepsilon_{zz}^a}{dx^4} = -\frac{1}{t_a}\left(\frac{1}{D_1}+\frac{1}{D_2}\right)\sigma_{zz}^a. \tag{7}$$

For symmetric joints Eq. (7) is further simplified to the following form:

$$\frac{d^4\varepsilon_{zz}^a}{dx^4} = -\frac{2}{t_a D_1}\sigma_{zz}^a. \tag{8}$$

Eq. (8) is the governing equation of the peel strain in the adhesive. Note that since the adhesive peel and shear strains (ε_{zz}^a) and (γ_{xz}^a) are computed from the relative displacements of the adherends [see Eqs. (1) and (6)], these quantities can be considered as the nominal (or averaged) values of the peel and shear strain through the adhesive thickness direction. Also note that the governing equations, Eqs. (4) and (8), are applicable to an adhesive with nonlinear constitutive behavior since no assumptions have yet been made to relate stresses and strains.

Adhesive Constitutive Behavior

Three-dimensional constitutive behavior of the adhesive in the elastic region is given in Eq. (9). E_a is the Young's modulus of the adhesive and ν is the Poisson's ratio. All stresses and strains with the superscript $\boldsymbol{a}$ are the adhesive stresses and strains:

$$\begin{Bmatrix} \sigma_{xx}^a \\ \sigma_{yy}^a \\ \sigma_{zz}^a \\ \tau_{yz}^a \\ \tau_{xz}^a \\ \tau_{xy}^a \end{Bmatrix} = \frac{E_a}{(1-2\nu)(1+\nu)} \begin{bmatrix} 1-\nu & \nu & \nu & 0 & 0 & 0 \\ \nu & 1-\nu & \nu & 0 & 0 & 0 \\ \nu & \nu & 1-\nu & 0 & 0 & 0 \\ 0 & 0 & 0 & \frac{1-2\nu}{2} & 0 & 0 \\ 0 & 0 & 0 & 0 & \frac{1-2\nu}{2} & 0 \\ 0 & 0 & 0 & 0 & 0 & \frac{1-2\nu}{2} \end{bmatrix} \times \begin{Bmatrix} \varepsilon_{xx}^a \\ \varepsilon_{yy}^a \\ \varepsilon_{zz}^a \\ \gamma_{yz}^a \\ \gamma_{xz}^a \\ \gamma_{xy}^a \end{Bmatrix}. \tag{9}$$

Generally, the adhesive normal stress, σ^a_{xx}, is very small compared with the other adhesive stress components, hence this stress component is assumed to be negligible [21,22]:

$$\sigma^a_{xx} = 0. \tag{10}$$

Eq. (9) can be further simplified by assuming plane strain conditions ($\varepsilon^a_{yy} = \gamma^a_{yz} = \gamma^a_{xy} = 0$).

$$\begin{Bmatrix} \sigma^a_{xx} \\ \sigma^a_{yy} \\ \sigma^a_{zz} \\ \tau^a_{yz} \\ \tau^a_{xz} \\ \tau^a_{xy} \end{Bmatrix} = \begin{Bmatrix} 0 \\ \dfrac{\nu E_a}{(1-\nu^2)}\varepsilon^a_{zz} \\ \dfrac{E_a}{(1-\nu^2)}\varepsilon^a_{zz} \\ 0 \\ G_a\gamma^a_{xz} \\ 0 \end{Bmatrix}, \tag{11}$$

where G_a is the shear modulus of the adhesive. Note that ε^a_{xx} is nonzero and can be related to the adhesive peel strain, ε^a_{zz}, *via* the plane strain assumption and Eq. (10).

$$\varepsilon^a_{xx} = -\frac{\nu}{1-\nu}\varepsilon^a_{zz}. \tag{12}$$

Therefore, the two remaining independent strain components appearing in Eq. (11) are the adhesive shear strain, γ^a_{xz}, and the adhesive peel strain, ε^a_{zz}.

The von Mises yielding criterion is used to define the yielded region of the adhesive. Von Mises effective stress can be expressed as a function of only the adhesive peel stress, σ^a_{zz}, and shear stress, τ^a_{xz}, by relating the stress component, σ^a_{yy}, to the peel stress, σ^a_{zz}, *via* the peel strain, ε^a_{zz}:

$$\sigma_{eff} = \sqrt{(\nu^2 - \nu + 1)(\sigma^a_{zz})^2 + 3(\tau^a_{xz})^2}. \tag{13}$$

It should be noted that the von Mises yield criterion accounts only for shear deformation processes and, thus, the analysis presented herein specifically does not include the effects of hydrostatic stress on the yielding behavior of the adhesive. This model was used due to its simplicity in the development of the closed-form solution presented herein. More complex yield criteria such as the Drucker-Prager models would need to be employed in order to account for the effects of combined deviatoric and hydrostatic stress components in the adhesive's yielding behavior.

Upon initial loading by the in-plane tension force, N_x, the adhesive shear and peel stresses developed in the adhesive are elastic until

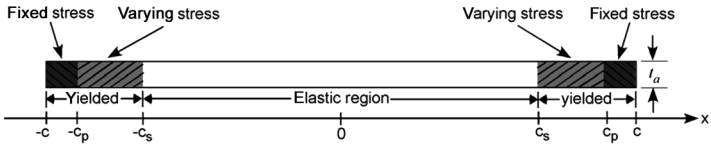

FIGURE 4 Adhesive yielded region divided into fixed stress and varying stress domains

the effective stress computed from Eq. (13) reaches the uniaxial yield stress (σ_Y). Due to the assumption of elastic-perfectly plastic adhesive behavior, the effective stress has a constant value of σ_Y inside the yielded region. The in-plane tension force corresponding to when the adhesive effective stress just reaches the yielding stress will be referred to as the first yielding load, N_x^1. Adhesive stress components at this loading level are σ_{zz}^1 and τ_{xz}^1, and will be defined as the first yielding point. Note that the exact values of σ_{zz}^1 and τ_{xz}^1 are dependent upon the joint geometry. As the loading increases, the size of the yielded region grows and expands into the elastic region (see Figure 1).

In order to model the complex adhesive behavior within the yielded region, as observed *via* nonlinear finite element models, and to satisfy global force equilibrium of the adhesive stress profiles, the variation of the adhesive stress components within the yielded region are modeled by dividing the yielded region into two domains: fixed stress and varying stress. The fixed stress domain is at the outermost portion of the adhesive, nearest to $x = \pm c$, as shown in Figure 4. Within the fixed stress domain, the adhesive peel and shear stress have static values σ_{zz}^1 and τ_{xz}^1 matching the first yielding point. Within the varying stress domain, the adhesive peel and shear stresses are different from σ_{zz}^1 and τ_{xz}^1. In both cases, the adhesive effective stress, σ_{eff} [Eq. (13)], is equal to the yield stress, σ_Y. The fixed stress domain is defined as $c_p \leq |x| \leq c$. The varying stress domain is defined as $c_s \leq |x| \leq c_p$. Both domains together define the yielded region. The details of computing the stresses and strains within these domains, the size of these domains (*i.e.*, c_s and c_p), and the stresses and strains within the elastic region are described in the following sections.

ELASTIC STRESS SOLUTION

Within the elastic region, the governing equations [Eqs. (4) and (8)] are written in terms of adhesive peel and shear strain components

(ε_{zz}^a and γ_{xz}^a) using the elastic constitutive relationships in Eq. (11).

$$\frac{d^4\varepsilon_{zz}^a}{dx^4} = -\frac{2E_a}{D_1 t_a(1-\nu^2)}\varepsilon_{zz}^a \tag{14}$$

$$\frac{d^2\gamma_{xz}^a}{dx^2} = \frac{G_a}{t_a}\left(\frac{2}{E_1 t_1} + \frac{t_1^2}{2D_1}\right)\gamma_{xz}^a \tag{15}$$

Eqs. (14) and (15) are solved for the adhesive peel strain, ε_{zz}^a, and adhesive shear strain, γ_{xz}^a, respectively:

$$\varepsilon_{zz}^a(x) = C_1 \cos\beta x \cosh\beta x + C_2 \sin\beta x \sinh\beta x, \tag{16}$$

$$\gamma_{xz}^a(x) = 2C_3 \cosh\lambda x, \tag{17}$$

where

$$\beta = \frac{1}{\sqrt{2}}\left[\frac{2E_a}{D_1 t_a(1-\nu^2)}\right]^{1/4}, \tag{18}$$

$$\lambda = \left[\frac{G_a}{t_a}\left(\frac{2}{E_1 t_1} + \frac{t_1^2}{2D_1}\right)\right]^{1/2}. \tag{19}$$

Note that Eqs. (16) and (17) account for the solutions being symmetric about $x = 0$. C_1, C_2, and C_3 in Eqs. (16) and (17) are constants that can be found from the boundary conditions at the right end of Adherend 1 at $x = c$.

$$M_1(c) = \frac{N_x t_1}{2} \tag{20}$$

$$Q_1(c) = 0 \tag{21}$$

$$N_1(c) = N_x \tag{22}$$

Eqs. (20) and (21) are related to peel strain, ε_{zz}^a, *via* Eq. (6) and beam moment and shear force to displacement relationships.

$$\left.\frac{d^2\varepsilon_{zz}^a}{dx^2}\right|_{x=c} = \frac{M_1(c)}{D_1 t_a} = \frac{N_x t_1}{2D_1 t_a} \tag{23}$$

$$\left.\frac{d^3\varepsilon_{zz}^a}{dx^3}\right|_{x=c} = \frac{Q_1(c)}{D_1 t_a} = 0 \tag{24}$$

Eq. (22) is related to shear strain, γ_{xz}^{a}, by Eq. (2).

$$\left.\frac{d\gamma_{xz}^{a}}{dx}\right|_{x=c} = \frac{N_x}{t_a}\left(\frac{1}{E_1 t_1} + \frac{t_1^2}{4D_1}\right) \tag{25}$$

These boundary conditions are applied to Eqs. (16) and (17) to determine C_1, C_2, and C_3.

$$\left\{\begin{array}{c} C_1 \\ C_2 \end{array}\right\} = \frac{N_x t_1}{2D_1 t_a \beta^2 (\sin 2\beta c + \sinh 2\beta c)} \left\{\begin{array}{l} \cos\beta c \sinh\beta c - \sin\beta c \cosh\beta c \\ \cos\beta c \sinh\beta c + \sin\beta c \cosh\beta c \end{array}\right\} \tag{26}$$

$$C_3 = \frac{N_x}{2\lambda t_a \sinh\lambda c}\left(\frac{1}{E_1 t_1} + \frac{t_1^2}{4D_1}\right) \tag{27}$$

The adhesive peel and shear stress elastic solutions are written as:

$$\sigma_{zz}^{a}(x) = \frac{E_a}{(1-\nu^2)}(C_1 \cos\beta x \cosh\beta x + C_2 \sin\beta x \sinh\beta x), \tag{28}$$

$$\tau_{xz}^{a}(x) = 2C_3 G_a \cosh\lambda x. \tag{29}$$

The elastic adhesive stresses given by Eqs. (28) and (29) are effective within the whole domain $-c \le x \le c$ as long as the applied tension force, N_x, is smaller than the first yielding load, N_x^1. N_x^1 is determined by using the maximum values of the adhesive peel and shear stresses [Eqs. (28) and (29) evaluated at $x = c$] to find the loading at which the adhesive effective stress, σ_{eff}, Eq. (13), is equal to the uniaxial yield stress, σ_Y:

$$N_x^1 = \sqrt{\frac{(\sigma_Y)^2}{(\kappa_1 + \kappa_2)}}, \tag{30}$$

where κ_1 and κ_2 are defined as

$$\kappa_1 = (\nu^2 - \nu + 1)\left[\frac{t_1 E_a}{4D_1 t_a \beta^2 (1-\nu^2)}\left(\frac{\sinh 2\beta c - \sin 2\beta c}{\sinh 2\beta c + \sin 2\beta c}\right)\right]^2, \tag{31}$$

$$\kappa_2 = 3\left[\frac{G_a \coth\lambda c}{\lambda t_a}\left(\frac{1}{E_1 t_1} + \frac{t_1^2}{4D_1}\right)\right]^2. \tag{32}$$

The adhesive stress components corresponding to the first yielding point are computed, using N_x^1, to be

$$\sigma_{zz}^1 = \frac{t_1 E_a}{4D_1 t_a \beta^2 (1-\nu^2)} \left(\frac{\sinh 2\beta c - \sin 2\beta c}{\sinh 2\beta c + \sin 2\beta c} \right) \sqrt{\frac{(\sigma_Y)^2}{(\kappa_1 + \kappa_2)}}, \tag{33}$$

$$\tau_{xz}^1 = \frac{G_a \coth \lambda c}{\lambda t_a} \left(\frac{1}{E_1 t_1} + \frac{t_1^2}{4D_1} \right) \sqrt{\frac{(\sigma_Y)^2}{(\kappa_1 + \kappa_2)}}. \tag{34}$$

ELASTO-PLASTIC STRESS SOLUTION

$N_x > N_x^1$, a yielded region develops in the adhesive starting at $x = \pm c$. The elastic governing equations [Eqs. (14) and (15)] can be still used within the elastic region $(-c_s \le x \le c_s)$; however, these equations cannot be immediately solved since the boundary conditions at the interface of the elastic region and the yielded region $(x = c_s)$ are unknown *a priori* without also solving for stresses in the yielded region. The stress components in the yielded region are related by the von Mises yielding criterion, given by Eq. (13), with σ_{eff} equal to the yield stress, σ_Y. Inside the fixed stress domain $(c_p \le |x| \le c)$, the adhesive stress components σ_{zz}^a and τ_{xz}^a are fixed to the first yielding point values σ_{zz}^1 and τ_{xz}^1. Inside the varying stress domain $c_s \le |x| \le c_p$, the relationship between adhesive stress components is defined by Eq. (13). If one of the adhesive stress components can be known in this region *a priori*, the other adhesive stress component can be computed from Eq. (13). The adhesive peel stress, σ_{zz}^a, in the varying stress domain is approximated for $N_x > N_x^1$ by the elastic peel stress profile given by Eq. (28). Since σ_{zz}^a is known in the varying stress domain, the adhesive shear stress, τ_{xz}^a, in this domain can be calculated based on Eq. (13),

$$\tau_{xz}^a = \sqrt{\frac{(\sigma_Y)^2 - (\nu^2 - \nu + 1)(\sigma_{zz}^a)^2}{3}} \quad \text{for } c_s \le |x| \le c_p. \tag{35}$$

Similar approaches for approximating the adhesive peel stress in the elasto-plastic adhesive problem have been made by Adams *et al.* [19] and Yang *et al.* [23]. However, the z-direction force equilibrium of the adhesive peel stress was not enforced in their analyses and the adhesive peel strain throughout the entire yielded region was computed based on elastic constitutive behavior. In the present analysis, the adhesive peel stress and strain are approximated by the elastic solution over a portion of the yielded region $(c_s \le |x| \le c_p)$. Furthermore,

the total peel stress profile, $\sigma^a_{zz}(x)$, is defined such that z-direction force equilibrium is correctly satisfied, specifically

$$\int_{-c}^{c} \sigma^a_{zz}(x)dx = 0. \tag{36}$$

In order to solve the governing equations [Eqs. (4) and (8)] within the yielded region, determination of the yielded region size (c_s) and the fixed stress domain size (c_p) is crucial. The size of the fixed stress domain (c_p) is determined based on observation of stress profiles calculated by nonlinear finite element models. These models and results are summarized in the Appendix. The elastic adhesive peel stress profile from Eq. (28), calculated for $-c \le x \le c$ at the given in-plane tension load N_x ($N_x > N_x^1$), has been truncated by the first yield adhesive peel stress, σ_{zz}^1, as can be seen in Figure 5. After c_p is determined from this truncation point, the adhesive peel stress profile within the region $-c_p \le x \le c_p$ is recalculated to satisfy Eq. (36) (solid line in Figure 5). The specific joint parameters for the calculations in Figure 5 are listed in the Appendix. N_x^1 is 107 N/mm for these specific joint parameters and N_x is chosen as twice the yielding load, N_x^1, in order to show the distinctive yielded regions which have initiated at the locations $x = \pm c$.

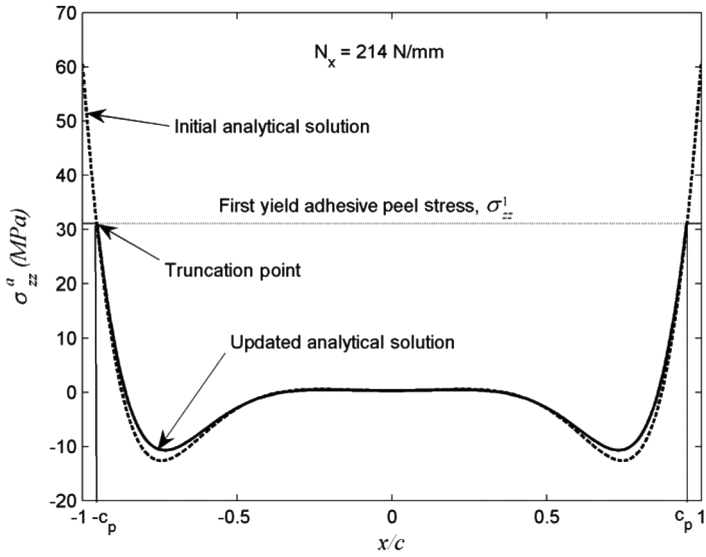

FIGURE 5 Computation of the size of fixed stress domain.

Note that the coefficients C_1 and C_2 must be updated to reflect the z-direction force equilibrium [Eq. (36)] and continuity of the adhesive peel stress profile at $x = c_p$. These updated C_1 and C_2 are defined as C_1^u and C_2^u. The adhesive peel stress, σ_{zz}^a, integrated from $-c$ to c should yield no net force. Inside the fixed stress domain ($c_p \leq |x| \leq c$), the adhesive peel stress is fixed to the first yield adhesive peel stress, σ_{zz}^1, and the integration of the adhesive peel stress inside this domain is $2\sigma_{zz}^1(c - c_p)$. Eq. (36) is rewritten using Eq. (28) within the region ($-c_p \leq x \leq c_p$):

$$\Omega_1 C_1^u + \Omega_2 C_2^u + 2\sigma_{zz}^1(c - c_p) = 0, \tag{37}$$

where

$$\Omega_1 = \frac{E_a}{(1-\nu^2)\beta}\left[\cos\beta c_p \sinh\beta c_p + \sin\beta c_p \cosh\beta c_p\right], \tag{38}$$

$$\Omega_2 = \frac{E_a}{(1-\nu^2)\beta}\left[\sin\beta c_p \cosh\beta c_p - \cos\beta c_p \sinh\beta c_p\right]. \tag{39}$$

The adhesive peel stress profile should be continuous inside the whole adhesive domain. Hence, the updated adhesive peel stress profile within $-c_p \leq x \leq c_p$ should have the same stress value, σ_{zz}^1, at the boundaries of the fixed stress domain $x = \pm c_p$. This condition is expressed as

$$\Omega_3 C_1^u + \Omega_4 C_2^u = \sigma_{zz}^1, \tag{40}$$

where

$$\Omega_3 = \frac{E_a}{(1-\nu^2)}\cos\beta c_p \cosh\beta c_p, \tag{41}$$

$$\Omega_4 = \frac{E_a}{(1-\nu^2)}\sin\beta c_p \sinh\beta c_p. \tag{42}$$

Eqs. (37) and (40) are solved simultaneously and the updated coefficients C_1^u and C_2^u are thereby determined.

$$\begin{Bmatrix} C_1^u \\ C_2^u \end{Bmatrix} = \frac{\sigma_{zz}^1}{\Omega_1\Omega_4 - \Omega_2\Omega_3}\begin{Bmatrix} 2\Omega_4(c_p - c) - \Omega_2 \\ 2\Omega_3(c - c_p) + \Omega_1 \end{Bmatrix} \tag{43}$$

In Figure 6, the analytically predicted adhesive peel stress profile is compared with the corresponding Finite Element Analysis (FEA) results. Details about the finite element model are given in the Appendix. The adhesive peel stress, σ_{zz}^a, is normalized by the yield stress, σ_Y.

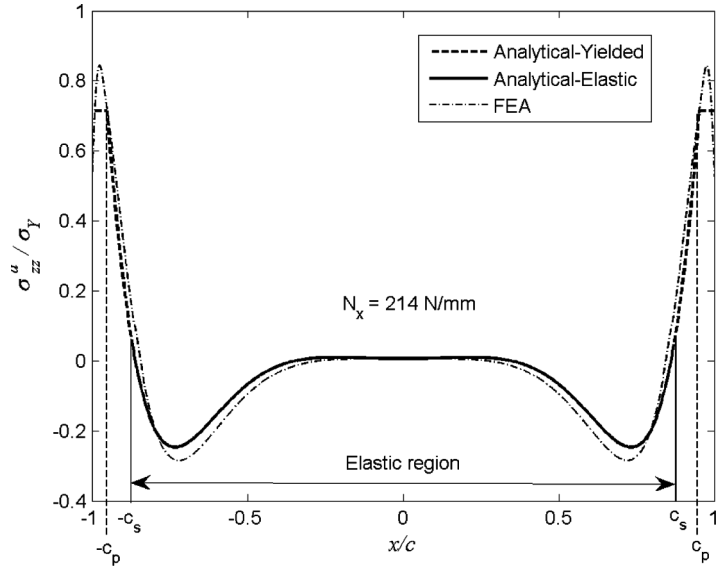

FIGURE 6 Adhesive peel stress predicted by analytical model and FEA.

The adhesive shear stress solution within the elastic region $(-c_s \leq x \leq c_s)$ can be computed using Eq. (29). Note that the adhesive shear stress solution within the varying stress domain $(c_s \leq |x| \leq c_p)$ is given by Eq. (35) since the peel stress profile is now established by Eq. (28) with the updated integration coefficients C_1^u and C_2^u given in Eq. (43). The integration coefficient C_3 used in Eq. (29) should also be updated to enforce continuity of the adhesive shear stress profile at $x = \pm c_s$. This updated C_3 is defined as C_3^u:

$$C_3^u = \frac{1}{2G_a \cosh \lambda c_s} \sqrt{\frac{(\sigma_Y)^2 - (\nu^2 - \nu + 1)(\sigma_{zz}^a|_{x=c_s})^2}{3}}. \tag{44}$$

C_3^u is found to be a function of the yielded region size, c_s, which is unknown *a priori*. The in-plane tension load being in equilibrium with the adhesive shear stress is used to establish another relationship between c_s and C_3^u.

$$\int_{-c}^{c} \tau_{xz}^a(x)dx = N_x. \tag{45}$$

Substituting Eqs. (29) and (35) into Eq. (45) and piecewise integrating over the half symmetric domain $0 \leq x \leq c$ yields the relationship

$$\int_0^{c_s} 2C_3^u G_a \cosh(\lambda x)dx + \int_{c_s}^{c_p} \tau_{xz}^a dx + \tau_{xz}^1 (c - c_p) = \frac{N_x}{2}. \qquad (46)$$

Note that the adhesive shear stress, τ_{xz}^a, is integrated numerically using the trapezoidal rule between c_s to c_p due to the difficult form of this function within the varying stress domain [see Eqs. (28) and (35)] not permitting exact closed-form integration. Two equations [Eqs. (44) and (46)] are used to determine the two unknowns C_3^u and c_s; since these equations cannot be solved explicitly because of the nonlinear terms in the equations, the following iterative method has been used:

1. Make initial guess for c_s ($0 \leq c_s \leq c_p$).
2. Compute C_3^u from the adhesive shear stress continuity condition [Eq. (44)].
3. Evaluate Eq. (46).
4. If Eq. (46) is not satisfied, the value of c_s should be changed.
5. Iterate this routine until Eq. (46) is satisfied.

In Figure 7, the analytically predicted adhesive shear stress profile is compared with the corresponding FEA results. Von Mises effective stress is computed using Eq. (13) and compared with corresponding

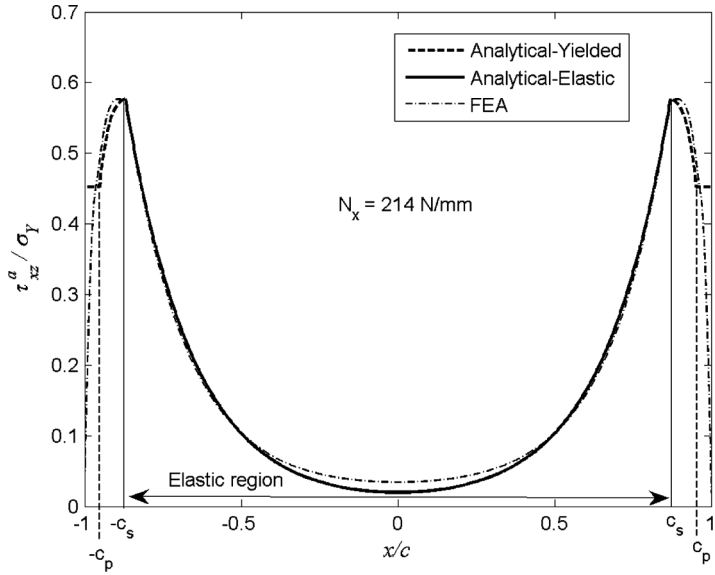

FIGURE 7 Adhesive shear stress predicted by analytical models and FEA.

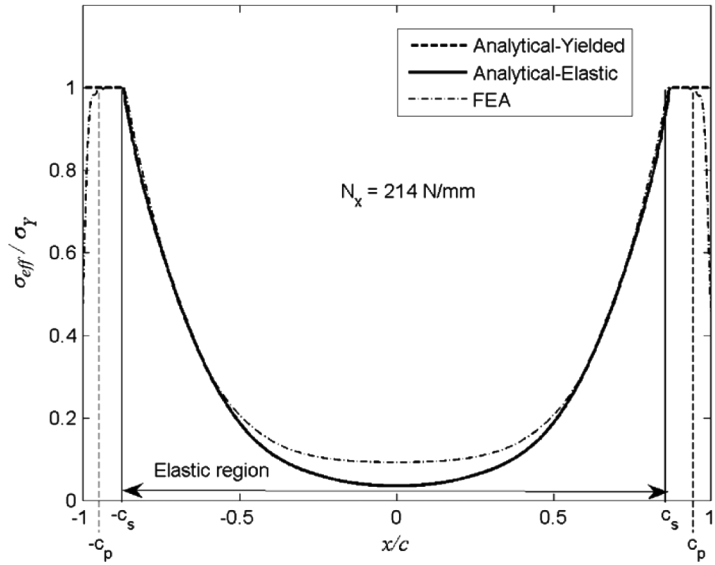

FIGURE 8 Von Mises effective stress predicted by analytical model and FEA.

FEA results in Figure 8. The analytical solution predicts peak shear stress magnitude and location very well with respect to the FEA results. Also, the effective stress profile in Figure 8 is well matched.

ADHESIVE STRAIN SOLUTIONS

Two strain components of interest within the adhesive are peel strain, ε^a_{zz}, and shear strain, γ^a_{xz}. These quantities must be computed separately within the different adhesive domains due to the nature of how yielding affects the mathematical form of the governing equations [Eqs. (4) and (8)]. Continuity conditions are enforced between the domains and serve as boundary conditions for these solutions.

Peel strain within the domain $-c_p \le x \le c_p$ can be calculated using Eq. (16) with updated coefficients C^u_1, C^u_2 [see Eq. (43)].

$$\varepsilon^a_{zz}(x) = C^u_1 \cos\beta x \cosh\beta x + C^u_2 \sin\beta x \sinh\beta x \quad \text{for } -c_p \le x \le c_p. \quad (47)$$

Within the domain $c_p \le |x| \le c$, peel strain must be determined by integrating Eq. (8). Recognizing that peel stress is fixed at σ^1_{zz} in this domain, the peel strain is

$$\varepsilon^a_{zz}(x) = -\frac{\sigma^1_{zz}}{t_a D_1}\frac{x^4}{12} + P_1\frac{x^3}{6} + P_2\frac{x^2}{2} + P_3 x + P_4 \quad \text{for } c_p \le |x| \le c. \quad (48)$$

The integration constants P_1 to P_4 are found *via* continuity of the peel strain solution at $x = c_p$, using Eq. (47) and derivatives evaluated at this location.

$$P_1 = \frac{2\sigma^1_{zz}c_p}{t_1 D_1} + 2\beta^3(-C^u_1 + C^u_2)\cos\beta c_p \sinh\beta c_p - 2\beta^3(C^u_1 + C^u_2)\sin\beta c_p \cosh\beta c_p \tag{49}$$

$$P_2 = \frac{\sigma^1_{zz}c_p^2}{t_1 D_1} - P_1 c_p - 2C^u_1\beta^2 \sin\beta c_p \sinh\beta c_p + 2C^u_2\beta^2 \cos\beta c_p \cosh\beta c_p \tag{50}$$

$$P_3 = \frac{\sigma^1_{zz}c_p^3}{3t_1 D_1} - \frac{P_1 c_p^2}{2} - P_2 c_p + (C^u_1 + C^u_2)\beta \cos\beta c_p \sinh\beta c_p + (C^u_2 - C^u_1)\beta \sin\beta c_p \cosh\beta c_p \tag{51}$$

$$P_4 = \frac{\sigma^1_{zz}c_p^4}{12t_1 D_1} - \frac{P_1 c_p^3}{6} - \frac{P_2 c_p^2}{2} - P_3 c_p + C^u_1 \cos\beta c_p \cosh\beta c_p + C^u_2 \sin\beta c_p \sinh\beta c_p \tag{52}$$

The peel strain solution [Eqs. (47) and (48)] plotted in Figure 9 is found to match FEA results closely.

Shear strain within the elastic domain $-c_s \le x \le c_s$ can be calculated using Eq. (17) with updated coefficients C^u_3 [see Eq. (44)].

$$\gamma^a_{xz}(x) = 2C^u_3 \cosh\lambda x \quad \text{for } -c_s \le x \le c_s. \tag{53}$$

The adhesive shear strain within the yielded region ($c_s \le |x| \le c$) cannot be analytically found and, thus, is computed by integrating Eq. 4 using Runge-Kutta fourth order numerical integration. The second order ordinary differential equation [Eq. (4)] is redefined as a linear system of two first order ordinary differential equations:

$$\gamma^a_{xz} = s_1, \tag{54}$$

$$\frac{d\gamma^a_{xz}}{dx} = s_2. \tag{55}$$

The adhesive shear strain governing equation within the yielded region becomes

$$s_2' = \frac{1}{t_a}\left(\frac{2}{E_1 t_1} + \frac{t_1^2}{2D_1}\right)\tau^a_{xz}(x) \quad \text{for } c_s \le |x| \le c. \tag{56}$$

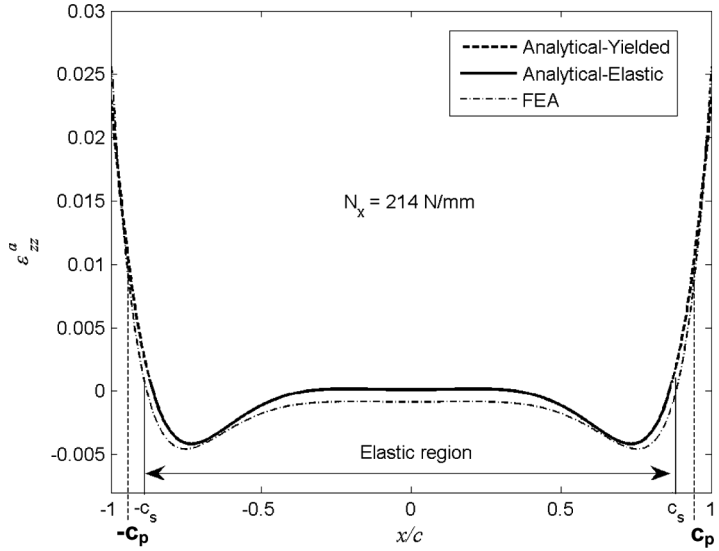

FIGURE 9 Adhesive peel strain predicted by analytical model and FEA.

Two initial conditions (s_1, s_2) are needed at $x = c_s$. These initial conditions can be obtained from Eq. (53) to enforce the continuity conditions of the adhesive shear strain profile at this location:

$$s_1|_{x=c_s} = 2C_3^u \cosh \lambda c_s, \tag{57}$$

$$s_2|_{x=c_s} = 2\lambda C_3^u \sinh \lambda c_s. \tag{58}$$

In Figure 10, the analytically predicted adhesive shear strain profile is compared with the corresponding FEA results. The effective strain can be computed by Eq. (59) as a function of adhesive peel and shear strain only:

$$\varepsilon_{eff} = \sqrt{\frac{2}{3}(\varepsilon_{zz}^a)^2 + \frac{1}{3}(\gamma_{xz}^a)^2}. \tag{59}$$

In Figure 11, the analytically predicted adhesive effective strain profile is compared with the corresponding FEA results.

The deviation of the shear and effective strain profiles from the FEA results is due to the basis of the analytical model on the shear lag and beam on elastic foundation formulations that compute strain from the relative adherend displacements. Therefore, the analytical model is not able to satisfy the traction-free boundary condition at the adhesive

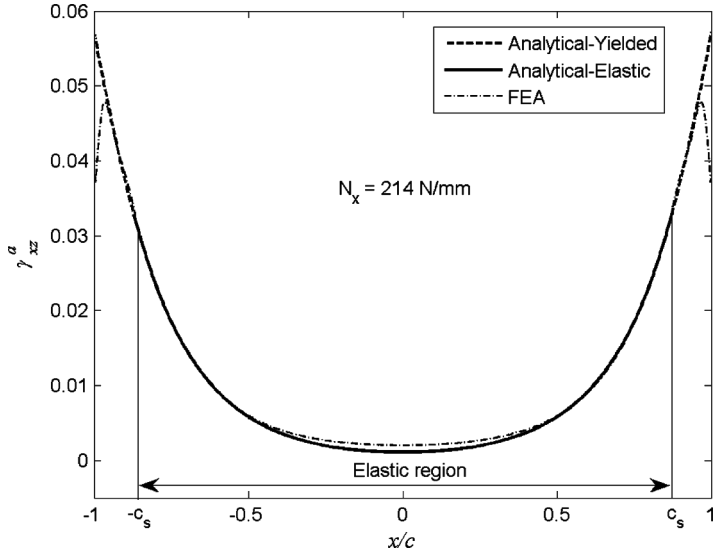

FIGURE 10 Adhesive shear strain predicted by analytical model and FEA.

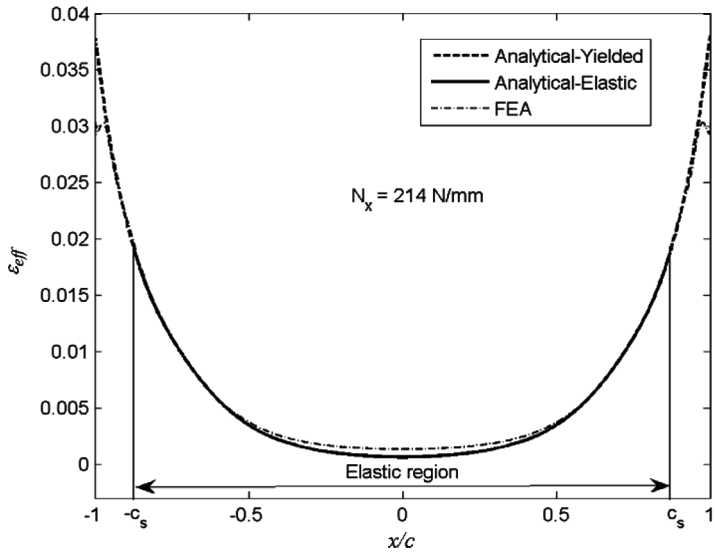

FIGURE 11 Effective strain predicted by analytical model and FEA.

free surfaces, and the strain localization at the joint interface corners. Both traction-free boundary condition and strain localization effects are captured by nonlinear FEA models having sufficient mesh refinement.

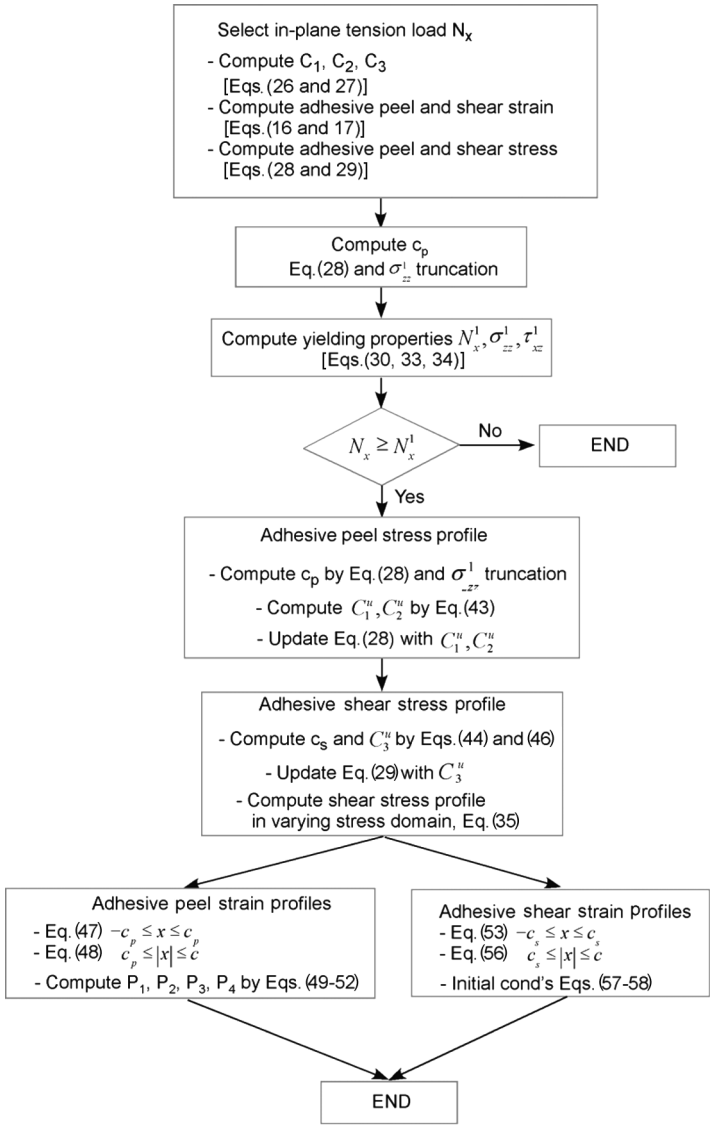

FIGURE 12 Algorithm for elasto-plastic analysis.

ANALYSIS PROCEDURE SUMMARY

The elasto-plastic analysis of bonded lap joints is summarized by the flow chart in Figure 12.

CASE STUDIES

The analytical model is demonstrated using two example case studies examining the variation of the adhesive thickness, t_a. Complementing the $t_a = 0.66$ mm adhesive thickness of the previous example calculations shown in Figures 5 to 11, these two studies have bondline thickness values of $t_a = 0.33$ and 1.02 mm. Parameters used in the calculations are listed in Table 1 while all adhesive and adherend material properties are given in the Appendix. Note that c_s and c_p are measured from the center of the joint.

For each case study, the normalized adhesive peel and shear stress profiles are plotted in Figures 13 to 18 and compared with corresponding FEA results taken along the adhesive midplane. The adhesive peel and shear strain profiles are also plotted in Figures 13 to 18 and compared with corresponding FEA results computed from the relative adherend displacements taken along the adhesive-adherend interfaces. Note that the FEA displacement readings (u, tangential and w, normal) always include the rigid body translations and rotations. These rigid body motions must be removed in post-processing to compute correctly the adhesive shear and peel strain [Eqs. (1) and (6)] from FEA. Load N_x is chosen as twice the yielding load, N_x^1, for each case study. In all FEA models, adhesive shear stress profiles satisfy the traction-free condition at both free surfaces of the adhesive (at $x = \pm c$) and, thus, to go zero. Note that this condition cannot be satisfied by the shear-lag based analytical model.

TABLE 1 Case Studies

Case study	Case I	Previous example calc.	Case II
c (mm)	12.7	12.7	12.7
t_a (mm)	0.33	0.66	1.02
N_x^1 (N/mm)	75	107	132
σ_{zz}^1 (MPa)	31.04	31.03	31.02
τ_{xz}^1 (MPa)	19.63	19.64	19.65
N_x (N/mm)	150	214	264
c_s (mm)	11.3	11.0	10.6
c_p (mm)	12.1	12.1	12.0

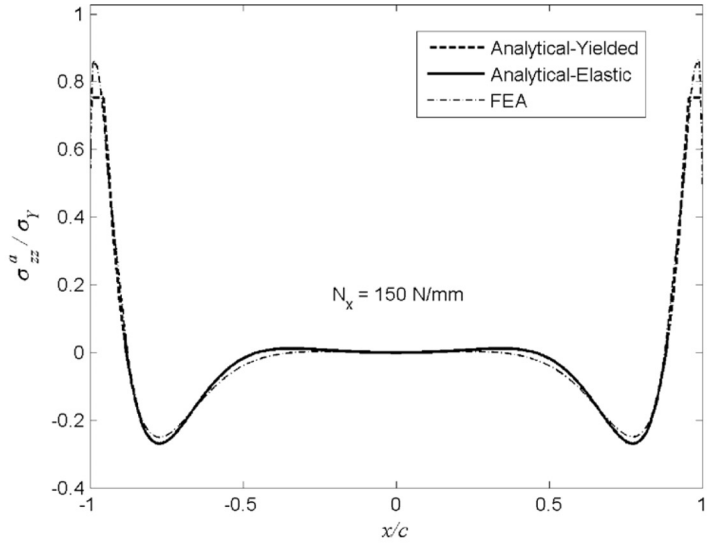

(a) adhesive peel stress

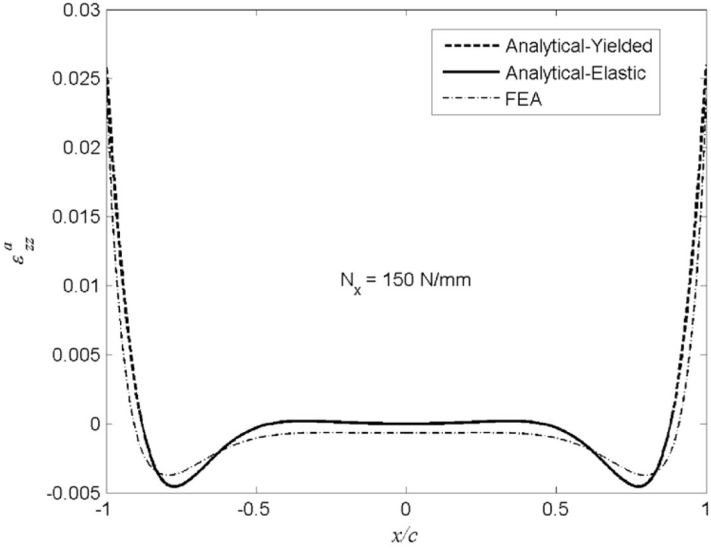

(b) adhesive peel strain

FIGURE 13 Case I adhesive peel stress and strain, $t_a = 0.33\,\text{mm}$, $c = 12.7\,\text{mm}$.

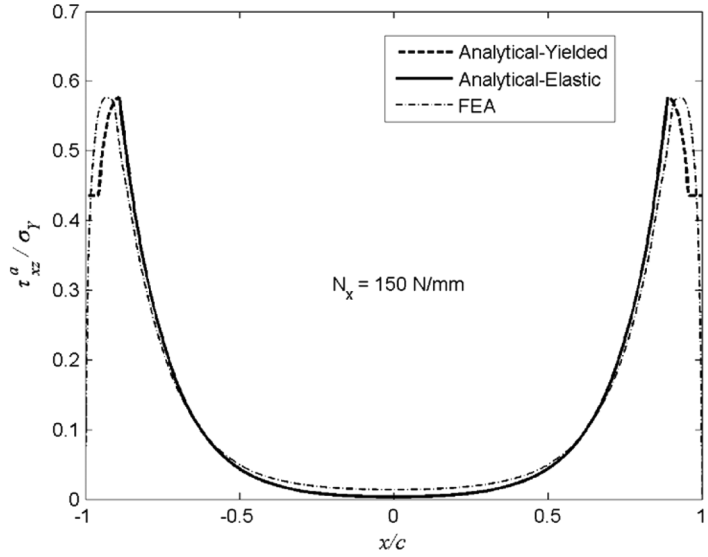

(a) adhesive shear stress

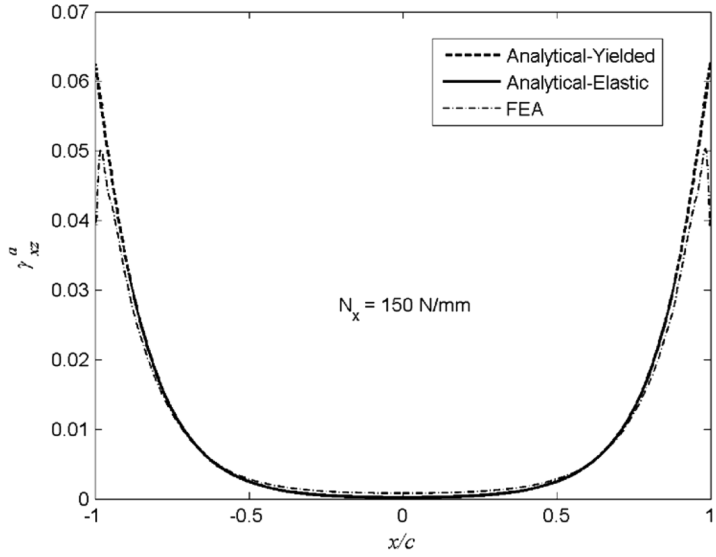

(b) adhesive shear strain

FIGURE 14 Case I adhesive shear stress and strain, $t_a = 0.33$ mm, $c = 12.7$ mm.

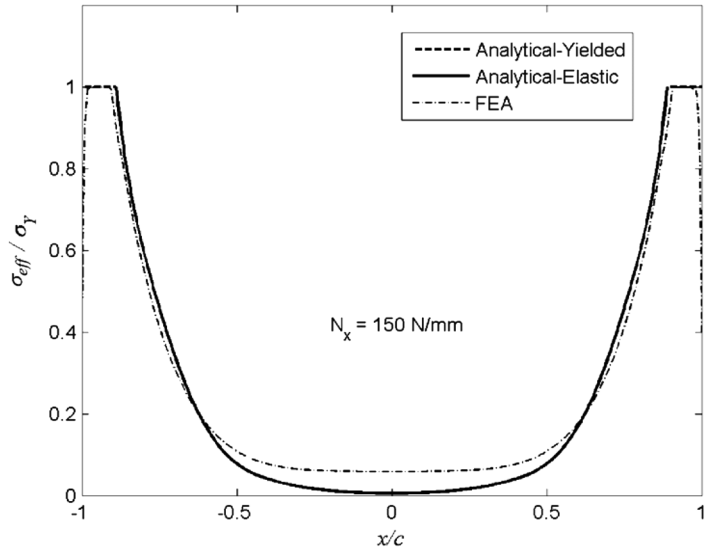

(a) effective stress

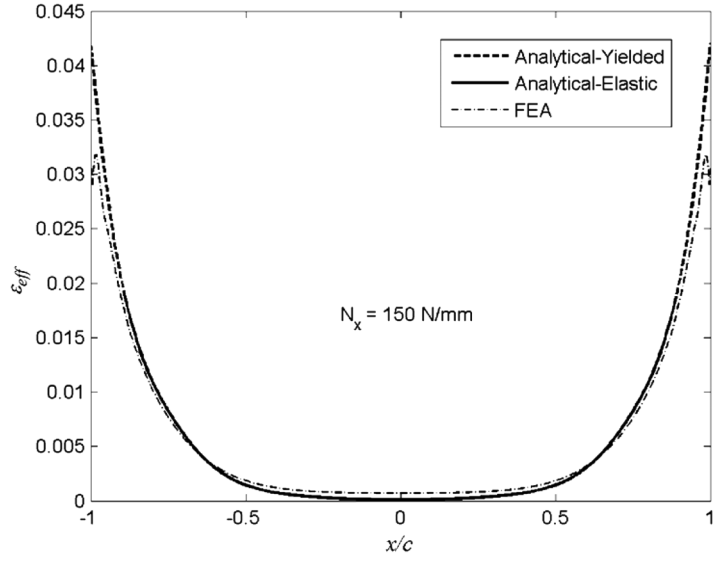

(b) effective strain

FIGURE 15 Case I adhesive effective stress and strain, $t_a = 0.33\,\text{mm}$, $c = 12.7\,\text{mm}$.

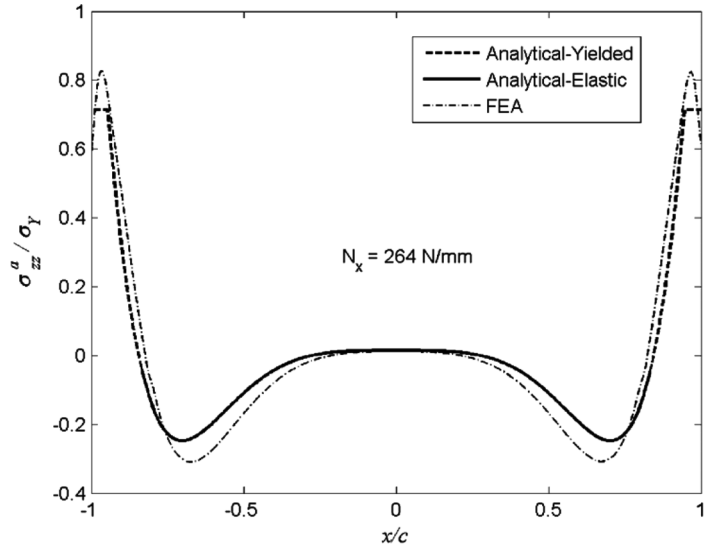

(a) adhesive peel stress

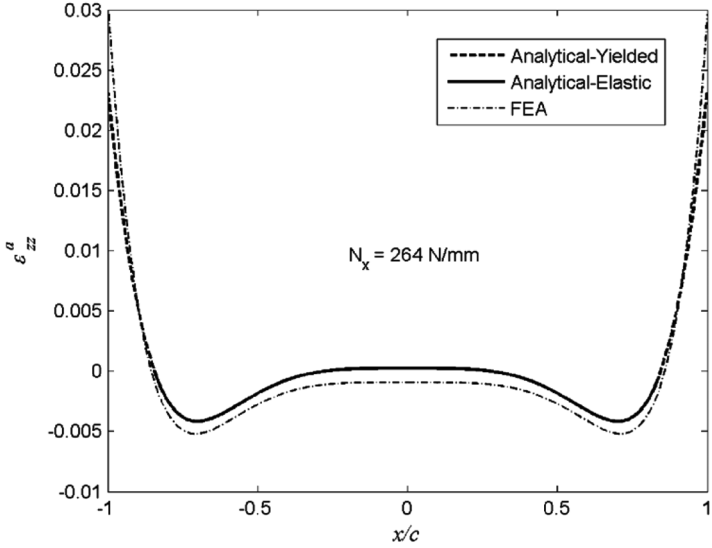

(b) adhesive peel strain

FIGURE 16 Case II adhesive effective peel stress and strain, $t_a = 1.02\,\text{mm}$, $c = 12.7\,\text{mm}$.

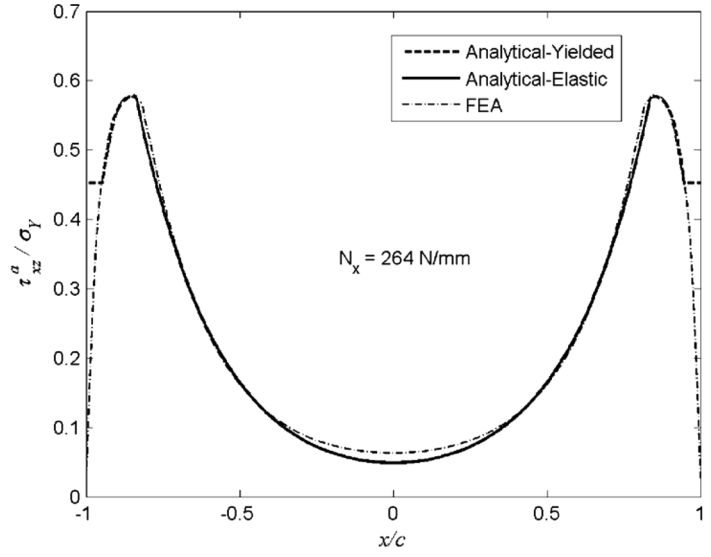

(a) adhesive shear stress

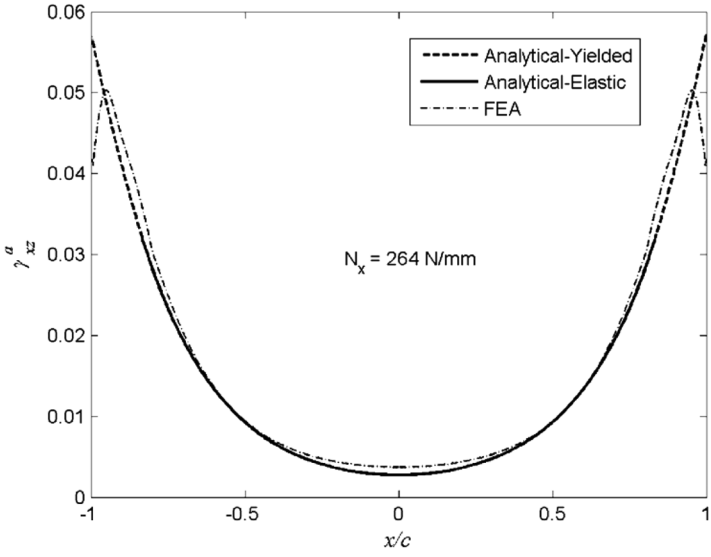

(b) adhesive shear strain

FIGURE 17 Case II adhesive shear stress and strain, $t_a = 1.02\,\text{mm}$, $c = 12.7\,\text{mm}$.

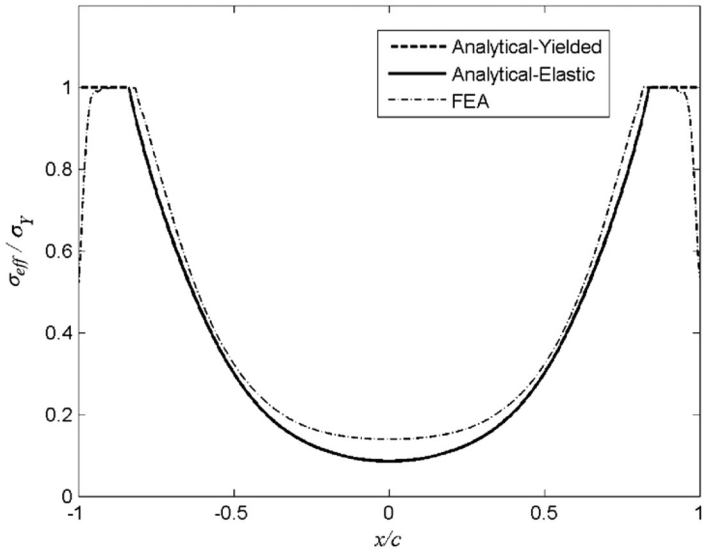

(a) effective stress

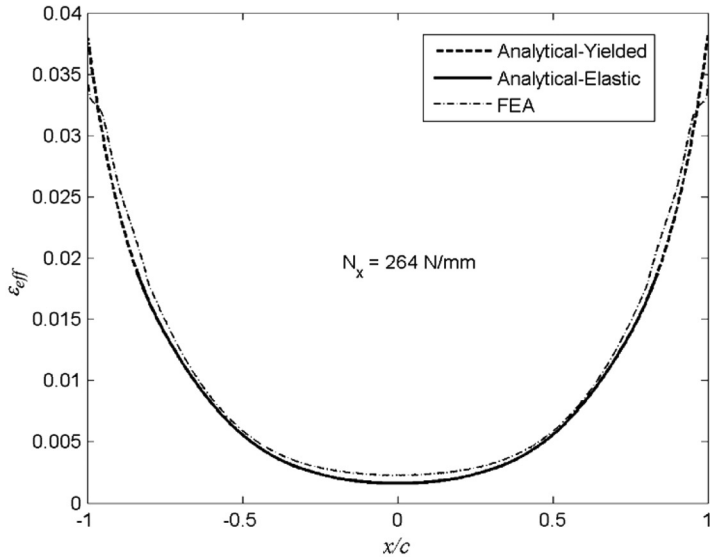

(b) effective strain

FIGURE 18 Case II adhesive stress and strain, $t_a = 1.02\,\text{mm}$, $c = 12.7\,\text{mm}$.

The case studies plotted in Figures 13 to 18 show that the analytical model is capable of predicting adhesive stress and strain quantities with reasonable accuracy over a range of bondline thickness. While the shear stress, τ^a_{xz}, and effective stress, σ_{eff}, magnitudes and profiles along the overlap were particularly well matched with FEA, the maximum peel stress was consistently under-predicted. Peel strain, ε^a_{zz}, was over-predicted for thin bondlines, but was under-predicted for $t_a = 1.02\,\text{mm}$, relative to FEA. This is due to the localization of plastic strain at the overlap interface corners, resulting in severely uneven distribution of strain in the though-bond-thickness direction that the FEA can predict, but the analytical models cannot. For the cases analyzed, maximum shear strain, γ^a_{xz}, was consistently over-predicted by the analytical model. Also, the maximum effective strain, ε_{eff}, was consistently over-predicted at $x = \pm c$. This is due to the analytical models being based on shear lag and beam on elastic foundation theories which are not able to capture the traction-free boundary condition at the ends of the joint. Therefore, using a failure criterion based on maximum effective strain would result in conservative failure load predictions.

CONCLUSIONS

An analytical model to predict the adhesive shear and peel stress and strain profiles for a symmetric single lap joint with elastic-to-perfectly plastic adhesive has been derived based on the shear lag and beam on elastic foundation models. The relationship between adhesive peel and shear stresses within the yielded region of the adhesive is found to be well described by the von Mises yielding criterion. The models predict the elastic-to-plastic transition location within the adhesive, and accurately predict shear stress to within 1% and peel stress to within 13%, for the case analyzed. The effective stress profile for all cases is almost identically predicted, relative to FEA, and the maximum effective strain is consistently over-predicted, which would result in conservative estimates of failure load when using an effective strain based failure criterion.

REFERENCES

[1] Volkersen, O., Die Niektraftverteilung in Zugbeanspruchten Nietverbindungen mit Konstanten Laschenquerschritten, *Luftfahrtforschung* **15**(1–2), 41–47 (1938).

[2] Hart-Smith, L. J., Adhesive-Bonded Double-Lap Joints, *NASA-Langley Contract Report*, NASA-CR-112235 (1973).

[3] Goland, M. and Reissner, E., The Stresses in Cemented Joints, *J. Applied Mechanics* **11**(1), A17–A27 (1944).

[4] Ojalvo, I. U. and Eidinoff, H. L., Bond Thickness Effects Upon Stresses in Single-Lap Adhesive Joints, *AIAA J.* **16**(3), 204–211 (1978).
[5] Oplinger, D. W., Effects of Adherend Deflections in Single Lap Joints, *Intern. J. Solids & Structures* **31**(18), 2565–2587 (1994).
[6] Kline, R. A., Stress Analysis of Adhesively Bonded Joints, *Proc. Intern. Symposium on Adhesive Joints*: *Characteristics and Testing*, September, 12–17, 1982 in Kansas City, MO, USA, pp. 587–610 (Plenum Press, NY). 1984.
[7] Delale, F., Erdogan, F., and Aydinoglu, M. N., Stresses in Adhesively Bonded Joints: A Closed form Solution, *J. Composite Materials* **15**, 249–271 (1981).
[8] Yang, C. and Pang, S., Stress-Strain Analysis of Single-Lap Joints Under Tension, *J. Engineering Materials & Technology* **118**(2), 247–255 (1996).
[9] Bigwood, D. A. and Crocombe, A. D., Elastic Analysis and Engineering Design Formulae for Bonded Joints, *Intern. J. Adhesion & Adhesives* **9**(4), 229–242 (1989).
[10] Mortensen, F. and Thomsen, O. T., Coupling Effects in Adhesive Bonded Joints, *Composite Structures* **56**(2), 165–174 (2002).
[11] Wu, Z. J., Romeijn, A., and Wardenier, J., Stress Expressions of Single-Lap Adhesive Joints of Dissimilar Adherends, *Composite Structures* **38**(1–4), 273–280 (1997).
[12] Lee, J. and Kim, H., Stress Analysis of Generally Asymmetric Single Lap Adhesively Bonded Joint, *J. Adhesion* **81**(5), 1–30 (2005).
[13] Kim, H., The Influence of Adhesive Bondline Thickness Imperfections on Stresses in Composite Joints, *J. Adhesion* **79**(7), 621–642 (2003).
[14] Tsai, M. Y., Oplinger, D. W., and Morton, J., Improved Theoretical Solutions for Adhesive Lap Joints, *Intern. J. Solids & Structures* **35**(12), 1163–1185 (1998).
[15] Nguyen, V. and Kedward, K. T., Non-Linear Modeling of Tubular Adhesive Scarf Joints Loaded in Tension, *J. Adhesion* **76**(3), 265–292 (2001).
[16] Kim, H. and Lee, J., Stress Adhesive Nonlinearity and the Prediction of Failure in Bonded Composite Lap Joints, in *Joining & Repair of Composite Structures, ASTM STP 1455*, K. T. Kedward and H. Kim (Eds.) (ASTM, Philadelphia, PA, USA, 2004), pp. 22–41.
[17] Hart-Smith, L. J., Adhesive-Bonded Single-Lap Joints, *NASA-Langley Contract Report*, NASA-CR-112236 (1973).
[18] Pickett, A. K. and Hollaway, L., The Analysis of Elastic-Plastic Adhesive Stresses in Bonded Lap Joints in FRP Structures, *Composite Structures* **4**(2), 135–160 (1985).
[19] Adams, R. D., Atkins, R. W., Harris, J. A., and Kinloch, A. J., Stress Analysis and Failure Properties of Carbon-Fibre-Reinforced-Plastic/Steel Double-Lap Joints, *J. Adhesion*, **20**(1), 29–53 (1986).
[20] Bigwood, D. A. and Crocombe, A. D., Non-Linear Adhesive Bonded Joint Design Analyses, *Intern. J. Adhesion & Adhesives* **10**(1), 31–41 (1990).
[21] Crocombe, A. D. and Bigwood, D. A., Development of a Full Elasto-plastic Adhesive Joint Design, *J. Strain Anal. for Engg. Design* **27**(4), 211–218 (1992).
[22] Thomsen, O. T., Elasto-Static and Elasto-Plastic Stress Analysis of Adhesive Bonded Tubular Lap Joints, *Composite Structures* **21**(44), 249–259 (1992).
[23] Yang, C., Huang, H., Tomblin, J. S., and Sun, W., Elastic-Plastic Model of Adhesive-bonded Single-Lap Composite Joints, *J. Composite Materials* **38**(4), 293–309 (2004).
[24] Tong, L., Bond Strength for Adhesive-Bonded Single-Lap Joints, *Acta Mechanica* **117**(1–4), 101–113 (1996).
[25] Tong, L., A Nonlinear Analysis of Adhesive Bonded Symmetric Lap Joints Using Shear Lag Model, *Transactions of the Canadian Society for Mechanical Engineering* **24**(1B), 207–213 (2000).

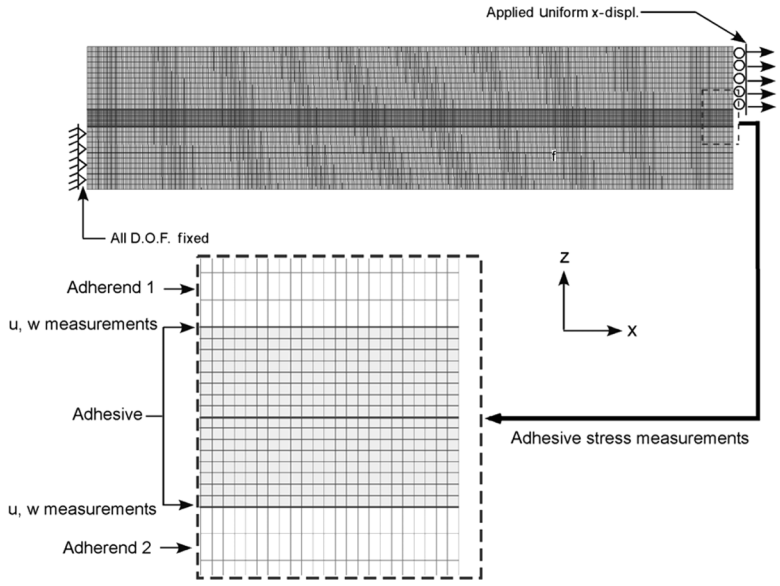

FIGURE A1 FEA mesh.

APPENDIX

FEA was conducted to assess analytical model accuracy and to justify the selection of the fixed stress domain size, c_p. The boundary conditions of the finite element model with the mesh are shown in Figure A1. Eight-noded plane strain elements with full-integration (CPE8) in ABAQUS/Standard v6.5–4 were used in this analysis. The joint parameters including specific constitutive behavior representing a structural epoxy adhesive (PTM&W ES6292 two-part paste

TABLE A1 Joint Parameters

Adhesive	E_a (GPa)	2.590
	G_a (GPa)	0.927
	ν	0.4
	t_a (mm)	0.66
	σ_Y (MPa)	43.46
Adherends	E_1 (GPa)	27.7
	t_1 (mm)	2.49
	D_1 (Nmm)	35.6×10^3
	$2c$ (mm)	25.4
Joint	N_x^1 (N/mm)	107
	σ_{zz}^1 (MPa)	31.03
	τ_{xz}^1 (MPa)	19.63

adhesive, PTM&W Industries, Santa Fe Springs, CA, USA) are listed in Table A1. These joint parameters were used for the example calculations shown in Figures 5 to 11. The adherends are 2.48 mm thick carbon/epoxy cloths of layup [0/45/–45/0].

The selection of c_p was motivated by the comparison of the adhesive peel stress profile between the nonlinear finite element model and the

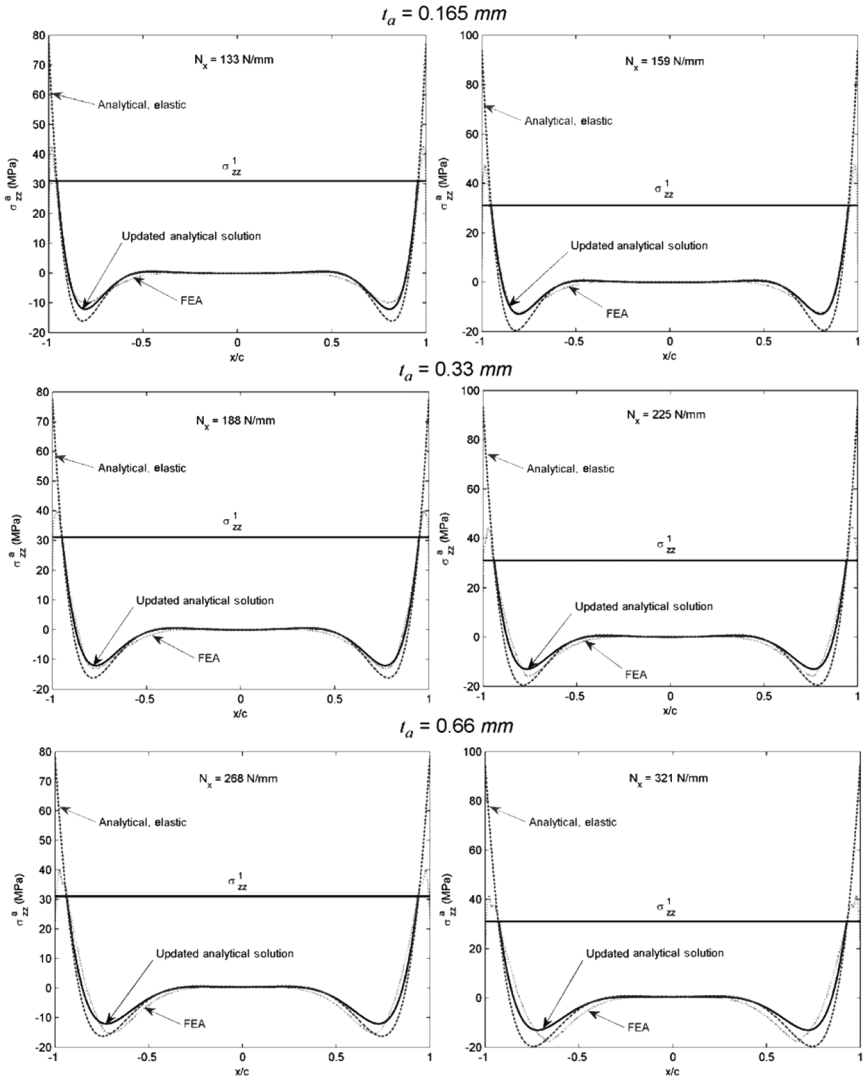

FIGURE A2 Determination of fixed stress domain size c_p.

elastic analytical model under wide variation of the adhesive thickness, t_a, and the in-plane tension load, N_x, which is chosen as 250% and 300% of N_x^1 (first yielding load) to cover a wide variation of in-plane force after yielding first occurs at N_x^1. In Figure A2, the adhesive peel stress profile from the initial analytical prediction with linear elastic adhesive property is plotted with the heavily dashed line, and the fine dashed line is the nonlinear FEA prediction. The crossing points of these two profiles are well approximated by the intersection of the first yield adhesive peel stress, σ_{zz}^1 (horizontal line), and the initial elastic solution, as can be seen in Figure A2 for a range of adhesive thickness. The solid line plotted in Figure A2 is the updated adhesive peel stress profile after the size of the fixed stress domain, c_p, is determined. The updated adhesive peel stress solution strictly satisfies the z-direction force equilibrium.